7.5

INSTABILITIES IN SWIRLING BOUNDARY LAYERS

David S. Nolan*
Division of Meteorology and Physical Oceanography
Rosenstiel School of Marine and Atmospheric Science, University of Miami, Florida

1. INTRODUCTION

Intense atmospheric vortices are the common feature of many important weather phenomena, occurring over wide scales from tornadoes to hurricanes to midlatitude cyclones. The interactions of these vortices with the surface (and humanity) is mediated by the swirling boundary layers which develop beneath them. Solutions describing such boundary layers, such as those from Ekman, Eliassen, and Von Karman, provide useful insight into their structure and behavior.

Observational, experimental, and numerical studies have shown that such swirling layers are generally unstable, and will develop quasi-streamwise rolls once they reach a sufficient intensity (Faller, 1963; Lilly, 1966; Savas, 1987; Lopez and Weidman, 1996; Wurman and Winslow, 1998; Montgomery et al., 2001). It is likely that these circulations enhance upward fluxes of heat and moisture from the surface (thereby influencing storm intensity) and also enhance downward fluxes of momentum toward the surface (thereby increasing damage potential).

These instabilities are analyzed using a model of linearized dynamics which allows for arbitrary structure of the axisymmetric vortex and its frictionally induced secondary circulation. The ultimate goal of this work will be the study of atmospheric vortices with stratification, spatially varying densities, and turbulent mixing. In the present work, we restrict our attention to swirling boundary layers beneath simple vortices with constant densities and eddy viscosities.

2. THE SYMMETRIC AND ASYMMETRIC TORNADO-HURRICANE EQUATIONS

Due to space limitations, we cannot provide a complete analysis of the equations, but we will instead describe the general approach; details are available in Nolan and Montgomery (2002b) and Nolan and Grasso (2003). We start from the anelastic momentum equations for dry adiabatic motions in cylindrical coordinates. These are comprised of the momentum equations for the radial (u), azimuthal (v), and vertical winds (w), the conservation of potential temperature (θ), and the anelastic (density weighted) incompressibility condition. For the puposes of generality, the effects of temperature and density variations and the earth's rotation are included in the present exposition. The equations are linearized for small perturbations about the basic-state flow, and these perturbations are assumed to have the form

$$v'(r, \lambda, z, t) = v_n(r, z, t)e^{in\lambda}, \qquad (1)$$

such that all variables vary exponentially in the azimuthal direction for some wavenumber n, but may have arbitrary structure in time and in the radial and vertical directions. After linearization and substitution for the perturbation variables in the form of (1), we have:

$$\frac{\bar{D}u_n}{Dt} + u_n\frac{\partial\bar{u}}{\partial r} + w_n\frac{\partial\bar{u}}{\partial z} - (2\bar{\Omega} + f)v_n = -\frac{1}{\bar{\rho}}\frac{\partial p_n}{\partial r}, \qquad (2)$$

$$\frac{\bar{D}v_n}{Dt} + w_n\frac{\partial\bar{v}}{\partial z} + \left(\frac{\partial\bar{v}}{\partial r} + \bar{\Omega} + f\right)u_n + \frac{\bar{u}}{r}v_n = -\frac{1}{\bar{\rho}}\frac{in}{r}p_n, \qquad (3)$$

$$\frac{\bar{D}w_n}{Dt} + u_n\frac{\partial\bar{w}}{\partial r} + w_n\frac{\partial\bar{w}}{\partial z} = -\frac{1}{\bar{\rho}}\frac{\partial p_n}{\partial z} + g\frac{\theta_n}{\bar{\theta}}, \qquad (4)$$

$$\frac{\bar{D}\theta_n}{Dt} + u_n\frac{\partial\bar{\theta}}{\partial r} + w_n\frac{\partial\bar{\theta}}{\partial z} = 0, \qquad (5)$$

$$\frac{1}{r\bar{\rho}}\frac{\partial}{\partial r}(r\bar{\rho}u_n) + \frac{in}{r}v_n + \frac{1}{\bar{\rho}}\frac{\partial}{\partial z}(\bar{\rho}w_n) = 0, \qquad (6)$$

where g is the gravitational acceleration, f is the Coriolis parameter, $\bar{\rho}$ is the (fixed) anelastic density field, p_n is the perturbation pressure, $\bar{\Omega} = \bar{v}/r$ is the basic-state angular velocity, and the basic-state material derivative is

$$\frac{\bar{D}}{Dt} = \frac{\partial}{\partial t} + \bar{u}\frac{\partial}{\partial r} + in\bar{\Omega} + \bar{w}\frac{\partial}{\partial z}. \qquad (7)$$

We refer to (2)-(7) as the *symmetric* (for $n = 0$) or *asymmetric* (for $n > 0$) *tornado-hurricane equations*. Since hurricanes can be represented to first order as a vortex in gradient wind and hydrostatic balance, with no secondary circulation, we call these equations with $\bar{u}(r, z) = \bar{w}(r, z) = 0$ the *symmetric/asymmetric hurricane equations*. Alternatively, since the dynamics of tornadoes are represented accurately by an incompressible vortex driven by overhead convection, we shall call the equations with $\bar{\rho}(r, z)$ constant, and (5) neglected, the *symmetric/asymmetric tornado equations*. Diffusion terms have been omitted here, but are included.

* Corresponding author address: Prof. David S. Nolan, RSMAS/MPO, University of Miami,
4600 Rickenbacker Causeway, Miami, FL 33149.
email: dnolan@rsmas.miami.edu

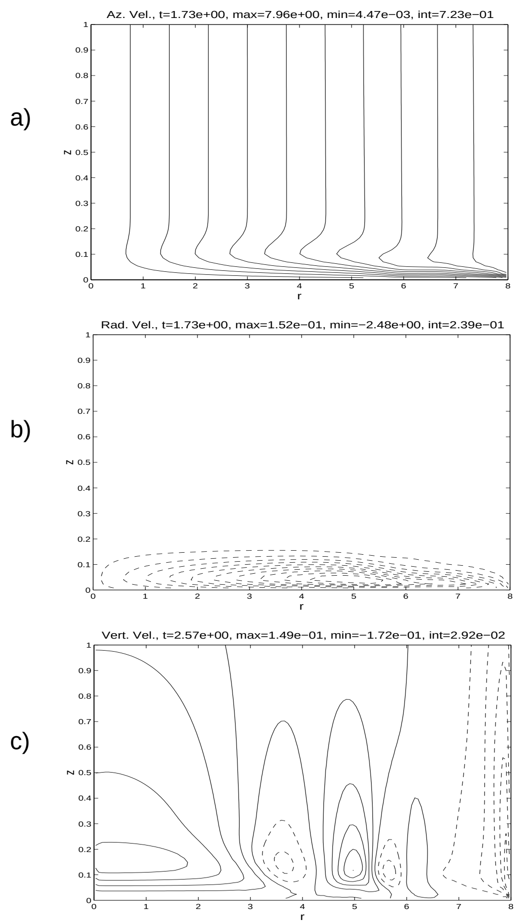

Figure 1: Swirling flow in the laboratory vortex:
a) Azimuthtal velocity at t = 1.73.
b) Radial velocity at t = 1.73.
c) Vertical velocity at t = 2.57.
Negative contours are dashed.

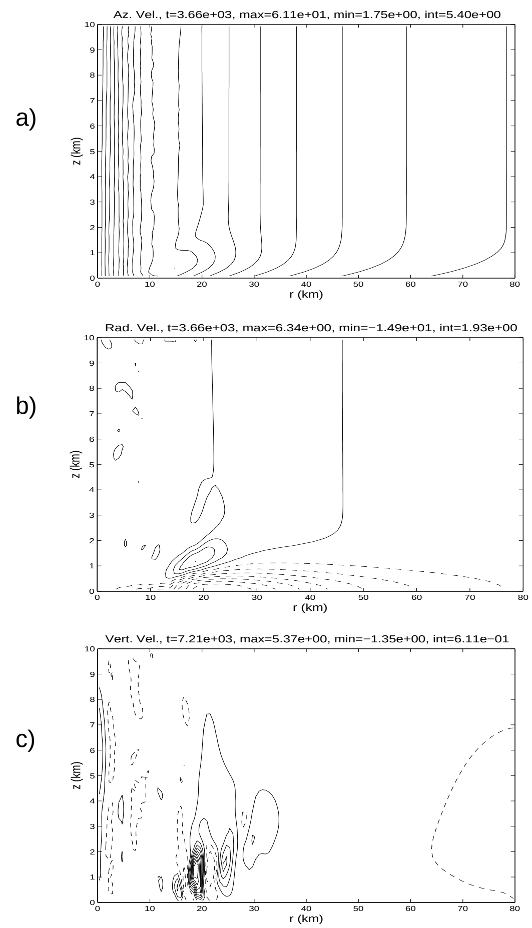

Figure 2: Swirling flow in the hurricane vortex.
a) Azimuthal velocity at t = 3660 s.
b) Radial velocity at t = 3660 s.
c) Vertical velocity at t = 7210 s.

For $n > 0$, observe that there are no derivatives operating on v_n in (6), such that v_n can be eliminated in favor of u_n and w_n. The same applies for p_n in (3), and thus p_n may also be eliminated. Through various manipulations we are left with three coupled, linear equations for u_n, w_n, and θ_n. Note that this approach cannot be used for $n = 0$; in this case, p_0 may be eliminated through the use of a streamfunction ψ_0, leading to three equations for ψ_0, v_0, and θ_0.

Here, we use the symmetric and asymmetric tornado equations exclusively, with $f = 0$. Similar analyses for tornado-like vortices were presented by Nolan and Montgomery (2002a). The effects of variable density and stratification remain for future work.

3. SWIRLING BOUNDARY LAYERS FROM AN AXISYMMETRIC MODEL

The swirling boundary layers are generated with a numerical model of axisymmetric, incompressible fluid flow (Nolan and Farrell, 1999). We consider two distinct cases. A “laboratory” vortex is created from the impulsive spindown of fluid in solid body rotation over a stationary lower surface with a no-slip boundary condition. The domain is a cylinder with a (dimensionless) radius R = 8.0 and height Z = 2.0. The fluid initially rotates at an angular velocity Ω = 1.0. The kinematic viscosity ν = 0.001. Free-slip boundary conditions are enforced at the other domain edges. A boundary layer quickly develops along the lower surface (Fig 1a, 1b). Shortly afterwards, axisymmetric roll instabilities appear near the outer wall and propagate into the domain (Fig 1c). It is worth noting that these waves appear almost immediately after the azimuthal wind field develops a low level jet, as indicated in Fig 1a. At later times, these rolls grow in number and intensity until the boundary layer is swamped with two-dimensional turbulence.

Following the work of Montgomery et al., 2001, the second swirling boundary layer is generated from the impulsive spindown of a “hurricane” vortex with an azimuthal wind profile modeled after a intense tropical cyclone:

$$v(r) = \frac{2r^* V_{\max}}{(1 + r^{*2})} \tag{8}$$

where $r^* = r/\mathrm{RMW}$, RMW = 12 km is the radius of maximum winds, and $V_{\max}$ = 60 ms^{-1}. This velocity profile has solid-body rotation in the core, transitioning to a $1/r$ profile in the far-field. The model domain extends to R = 80 km and Z = 10 km. The vortex interacts with a “semi-slip” lower boundary condition commonly used in meterological modeling to represent the stress caused by turbulent drag over a rough surface, i.e.,

$$\tau_{[u,v]} = C_d \times [u, v] \times V \qquad (9)$$

where V is the absolute wind speed at the surface and C_d is a drag coeffcient set to a typical value of 0.002. The internal eddy viscosity ν = 100 m^{2}s^{-1}. This boundary layer is a little more complicated, with maximum radial inflow and vertical motion appearing near the radius of maximum winds as predicted by Eliassen (1971) (Fig. 2a). In contrast with the “laboratory” vortex, there is also a significant outward return flow just above the boundary layer near the RMW (Fig. 2b). As time evolves, axisymmetric rolls develop in this region and propagate inward at approximately 4 ms^{-1} (Fig. 2c).

4. NUMERICAL SOLUTION

The symmetric and asymmetric tornado equations are discretized onto an Arakawa-C grid in the r,z plane. Through standard techniques the linear equations may be transformed into the linear dynamical system

$$\frac{d\mathbf{x}_n}{dt} = \mathbf{T}_n \mathbf{x}_n \,, \qquad (10)$$

where $\mathbf{x}_n$ is a column vector whose elements contain the values of each free variable at each gridpoint. The eigenvectors of the matrix $\mathbf{T}_n$ are the modes of the system.

Some practical difficulty lies in the size of the matrix $\mathbf{T}_n$. Using a regularly spaced grid, one might need as many as 100 points in each of the radial and vertical directions for sufficient resolution of the boundary layers. The size of $\mathbf{T}_n$ would then be on the order of 20000x20000. To overcome this difficulty we use grids that are stretched in both the radial and vertical directions, such that a large number of gridpoints are packed into the lower levels of the inner core of the vortex. For the laboratory vortex, the gridpoints are not stretched radially. In both cases, there are 35 points in the radial direction and 50 points in the vertical direction. The minimum vertical grid spacing is Δz = 0.0147 for the laboratory vortex and Δz = 97 m for the hurricane vortex.

5. UNSTABLE MODES IN THE LABORATORY VORTEX

The basic-state to be studied is generated from a time average of the swirling flow from shortly before to shortly after the appearance of the axisymmetric instabilities. For n = 0 (axisymmetric modes), the most unstable mode is found to have an e-folding time of 1.24 (dimensionless) time units. The real and imaginary parts of this mode are shown in Fig. 3a and 3b. The existence of complex values in this eigenvector and its associated eigenvalue are indicative of an apparent inward propagation of the phase lines of the growing mode. [The physical solution is the real part of $w_n e^{st}$, where s is the complex eigenvalue. For Re{s} > 0, the physical solution evolves as Re{w_n} --> -Im{w_n} --> -Re{w_n} --> Im{w_n}.] However, asymmetric modes for n = 1 grow slightly faster, with an e-folding time of 1.12. A horizontal cross-section of this mode is shown in Fig 3c. Interestingly, this mode spirals in the “wrong” direction, at an angle to the shear vector. Such modes have indeed been observed in laboratory experiments (Faller, 1963; Savas, 1987). Other unstable eigenmodes for this flow, with growth rates nearly as large as the most unstable more, did spiral in the same sense of the flow. Energetic analyses for these symmetric and asymmetric instabilities find that 80-90% of the basic-state to perturbation energy conversion is associated with the vertical shear of the azimuthal wind.

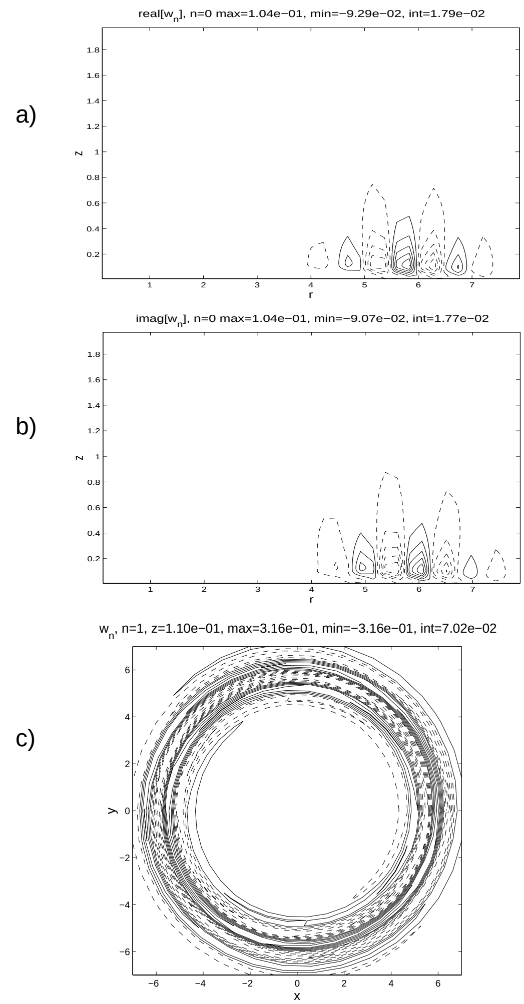

Figure 3: Most unstable modes in the laboratory vortex.
a) Real part of w for n = 0.
b) Imaginary part of w for n = 0.
c) Horizontal cross section (real part) for n =1.

The analyzed instabilities have shorter radial wavelengths than those seen in the axisymmetric numerical simulation. However, the modes in the simulations are clearly excited by the recirculating corner flow at the outer edge of the domain (see Fig 1c), and thus may be biased toward larger scales.

6. UNSTABLE MODES IN THE HURRICANE VORTEX

This analysis was repeated for the hurricane vortex swirling boundary layer. As the lower boundary condition for this flow is nonlinear and inhomogeneous, the lower boundary conditions for the linear modes were made free slip as a first approximation to a semi-slip boundary condition with a low drag coefficient. For $n = 0$, the most unstable mode has an *e*-folding time of 0.36 h; its real and imaginary parts are shown in Fig 4a and 4b. As in the nonlinear simulations, the unstable waves are found to propagate inward, but at a much faster speed of about 10 ms^{-1}. Asymmetric modes are again more unstable; for $n = 1$, the *e*-folding time is 0.29 h, with a “reverse” spiral structure as shown in Fig 4c. For these modes (symmetric and asymmetric), approximately half the energy conversion is associated with each of the vertical and radial shears of the azimuthal wind, indicating that the instability mechanism may be of a different nature than for the laboratory vortex. However, these results should be viewed with caution until a lower boundary condition can be implemented for the linear model which more accurately reflects the semi-slip drag law (9).

a)

b)

c)

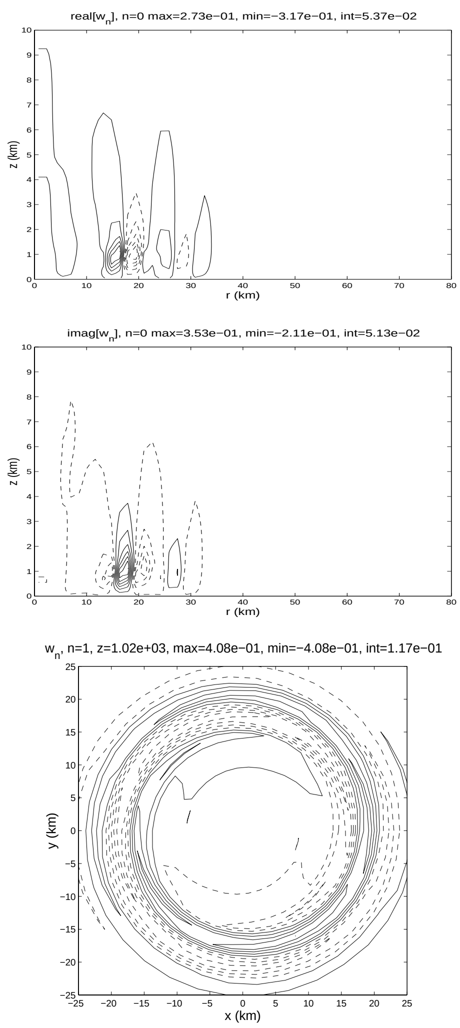

Figure 4: Most unstable modes in the hurricane vortex.
a) Real part of w for $n = 0$.
b) Imaginary part pf w for $n = 0$.
c) Horizontal cross section (real part) for $n = 1$.

7. CONCLUSIONS

This work represents a step further toward a thorough understanding of the dynamics of instabilities in the boundary layers of atmospheric vortices. For simple vortices in incompressible fluid flows, the linear model recovers the instabilities suggested by both numerical simulations and observations. Preliminary analyses indicate the instabilities in the hurricane-like vortex are quite different from those in the laboratory spin-down experiments. Future work will extend this approach to fully compressible, stratified flows, using the complete symmetric and asymmetric tornado-hurricane equations.

8. ACKNOWLEDGEMENTS:

This work was supported by the NSF under grant ATM-0132006 and by the University of Miami.

REFERENCES:

Eliassen, A., 1971: On the Ekman layer in a circular vortex. *J. Met Soc. Japan*, **49**, 784-789.

Faller, A. J., 1963: An experimental study of hte instability of the laminar Ekman boundary layer. *J. Fluid Mech.*, **15**, 560-576.

Lilly, D. K., 1966: On the instability of the Ekman boundary layer flow. J. Atmos. Sci., 23, 481-494.

Lopez, J. M., and P. D. Weidman, 1996: Stability of stationary endwall boundary layers during spin-down. *J. Fluid Mech.,* **326**, 373-398.

Montgomery, M. T., H. D. Snell, and Z. Yang, 2001: Axisymmetric spindown dynamics of hurricane-like vortices. *J. Atmos. Sci.*, **58**, 421-435.

Nolan, D. S., and B. F. Farrell, 1999: The structure and dynamics of tornado-like vortices. *J. Atmos. Sci.*, **56**, 2908-2936.

Nolan, D. S., and L. D. Grasso, 2003: Three-dimensional, nonhydrostatic perturbations to balanced, hurricane-like vortices. Part II: Symmetric response and nonlinear simulations. To appear in *J. Atmos. Sci.*

Nolan, D. S., and M. T. Montgomery, 2002a: Three-dimensional stability analyses of tornado-like vortices with secondary circulations. *Preprints, 21st Conference on Severe Local Storms, San Antonio, TX, August 2002*. Amer. Met. Soc.

Nolan, D. S., and M. T. Montgomery, 2002b: Three-dimensional, nonhydrostatic perturbations to balanced, hurricane-like vortices. Part I: Linearized formulation, stability, and evolution. *J. Atmos. Sci.*, **59**, 2989-3020.

Savas, O., 1987: Stability of Bodewadt flow. *J. Fluid Mech*., **183**, 77-94.

Walko, R., and Gall, R., 1984: A two-dimensional linear stability analysis of the multiple vortex phenomena. *J. Atmos. Sci.*, **41**, 3456-3471.

Wurman, J., and J. Winslow, 1998: Intense sub-kilometer-scale boundary layer rolls observed in Hurricane Fran. *Science*, **280**, 555-557.